

## Inhibitors of Bacterial Cystathionine $\beta$ -Lyase: Leads for New Antimicrobial Agents and Probes of Enzyme Structure and Function

Linda J. Ejim, Jan E. Blanchard, Kalinka P. Koteva, Rachael Sumerfield, Nadine H. Elowe, Jonathan D. Chechetto, Eric D. Brown, Murray S. Junop, and Gerard D. Wright\*

Antimicrobial Research Centre, McMaster High Throughput Screening Laboratory, Department of Biochemistry and Biomedical Sciences, McMaster University, Ontario L8N 3Z5, Canada

Received September 28, 2006

The biosynthesis of methionine is an attractive antibiotic target given its importance in protein and DNA metabolism and its absence in mammals. We have performed a high-throughput screen of the methionine biosynthesis enzyme cystathionine  $\beta$ -lyase (CBL) against a library of 50 000 small molecules and have identified several compounds that inhibit CBL enzyme activity in vitro. These hit molecules were of two classes: those that blocked CBL activity with mixed steady-state inhibition and those that covalently interacted with the enzyme at the active site pyridoxal phosphate cofactor with slow-binding inhibition kinetics. We determined the crystal structure of one of the slow-binding inhibitors in complex with CBL and used this structure as a guide in the synthesis of a small, focused library of analogues, some of which had improved enzyme inhibition properties. These studies provide the first lead molecules for antimicrobial agents that target cystathionine  $\beta$ -lyase in methionine biosynthesis.

### Introduction

The continuous emergence of antibiotic resistance in microbial pathogens requires a sustained effort to identify new antimicrobial compounds and new targets. Traditional targets such as the cell wall, nucleic acid, and protein synthesis remain robust candidates; however, these likely under-represent the potential targets available for antibiotic discovery. As a result, there has been a call for exploration and screening of non-canonical targets in antimicrobial drug discovery.<sup>1,2</sup> Microbial amino acid biosynthesis is critical to cellular growth and therefore is an excellent candidate target for antimicrobial agents.<sup>3</sup> Under conditions of systemic infection, amino acid concentrations are generally low (e.g., in serum<sup>4</sup>) and unable to support microbial growth. As a result, the biochemical pathways that catalyze amino acid production are engaged to meet the anabolic requirements of the infectious cell. Microarray analysis of gene expression profiles of *Escherichia coli* growing in minimal versus rich media confirms that amino acid biosynthesis pathways are up-regulated during logarithmic and stationary growth phases under conditions of low amino acid availability.<sup>5</sup> Furthermore, proteomic analysis of genes expressed in typhoid fever and enteritis models of *Salmonella enterica* infection has shown that enzymes required for the biosynthesis of several amino acids such as methionine are expressed during infection.<sup>6</sup>

The potential of amino acid biosynthesis as an antimicrobial target has been validated both chemically and biochemically. For example, the antimicrobial compounds rhizocitin,<sup>7</sup> azoxybacilin,<sup>8</sup> 2-amino-5-hydroxy-4-oxopentanoic acid,<sup>9,10</sup> and (6S)-6-fluoroshikimic acid<sup>11</sup> target various bacterial and fungal amino acid biosynthetic enzymes and gene expression. Furthermore, mutants in amino acid biosynthetic genes in both bacteria and fungi are impaired in their ability to cause disease.<sup>12–15</sup>

Methionine biosynthesis is an especially attractive target in this regard. Methionine is not only required for the synthesis of proteins but also vital to C1 metabolism via the synthesis of

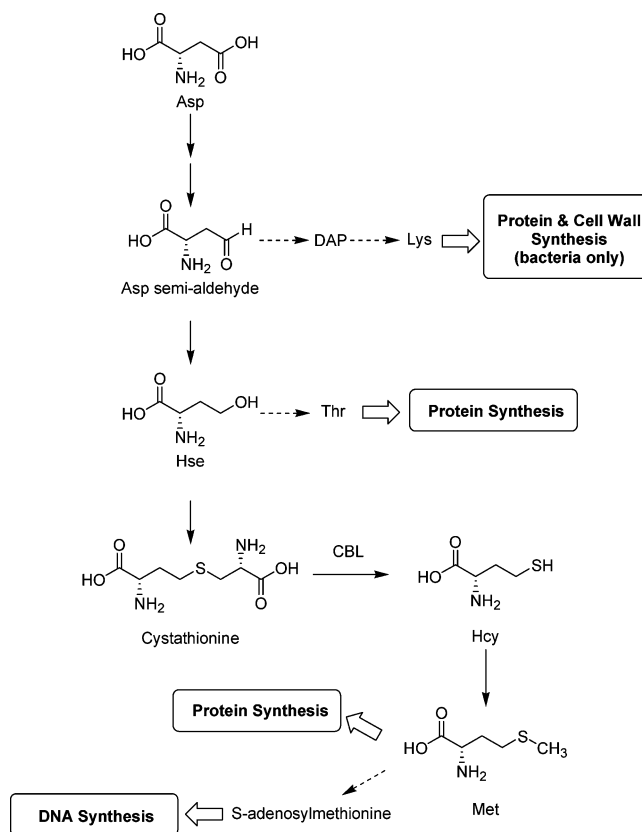
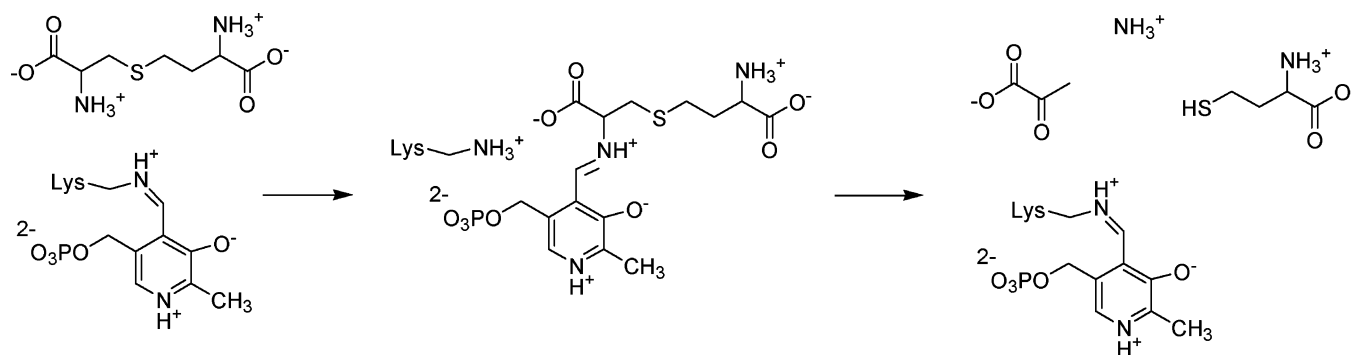


**Figure 1.** Biosynthesis of Met from the precursor Asp is vital to microbial protein and DNA metabolism.

the methyl donor *S*-adenosylmethionine and is thus directly linked to DNA replication through thymine biosynthesis (Figure 1). Inhibitors of methionine biosynthesis therefore have the potential to impact both DNA and protein synthesis simultaneously, thereby amplifying their toxic effects. Moreover, most of the steps in this pathway are absent in mammals, lessening the opportunity of unwanted toxic side effects. The antifungal

\* Corresponding Author. Phone: 905-525-9140 ex 22454. Fax: 905-522-9033. E-mail: wrightge@mcmaster.ca.

## Scheme 1



agents azoxybacilin<sup>8</sup> and 2-amino-5-hydroxy-4-oxopentanoic acid<sup>9</sup> target this pathway, and mutants in the genes encoding the biosynthetic enzymes have been shown to be avirulent in both bacteria and fungi.<sup>13,15</sup>

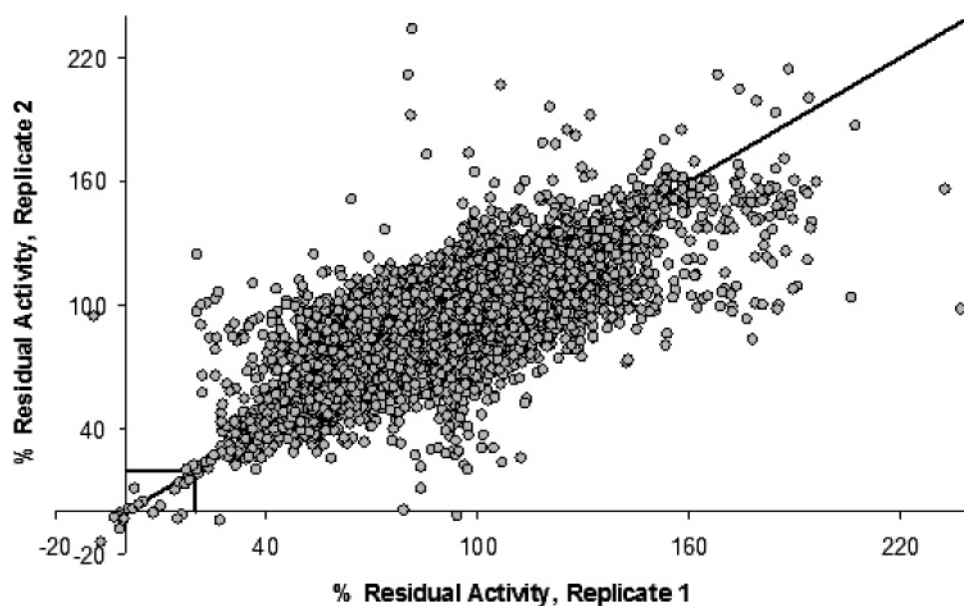
We have explored the importance of one of the enzymes required for methionine biosynthesis, cystathionine  $\beta$ -lyase (CBL,<sup>a</sup> encoded by *metC*), in bacterial infection by deleting the gene in *Salmonella enterica* serovar typhimurium and have demonstrated that the absence of *metC* attenuates virulence in a mouse model of systemic infection.<sup>12</sup> CBL is a ubiquitous microbial enzyme that cleaves cystathionine, generating ammonia, pyruvate, and homocysteine, the penultimate step in methionine biosynthesis (Scheme 1). Literature precedent linked the antifungal activity of anilinopyrimidine antifungal agents such as pyrimethanil to the inhibition of CBL;<sup>16</sup> however, we have not observed direct inhibition of the purified enzyme with these compounds.<sup>12</sup> Nevertheless, encouraged by our experiments linking CBL to bacterial virulence and because chemical inhibitors of enzymes in methionine biosynthesis can have antimicrobial activity as discussed above, we reasoned that a high-throughput screen of CBL could identify small molecules that could serve as enzyme probes or leads in antimicrobial agent development. Given that the enzyme requires an electrophilic pyridoxal phosphate (PLP) cofactor for catalysis, we designed the high-throughput assay to include a preincubation period with potential inhibitors to specifically ensure that compounds with slow-binding properties could be identified in the screen.

## Results

**High-Throughput Screen of CBL.** We screened *E. coli* CBL in duplicate against a 50 000-compound small-molecule library from Maybridge Plc. to identify potential inhibitory molecules. The  $Z'$  factor for the screen, a statistical measure of the effective separation of the high and low controls, was 0.54, indicating that this assay was highly suitable for screening.<sup>17</sup> Figure 2 shows a plot of the residual activities of the duplicate screen. We set the hit cut off at 20%, which resulted in 28 potential hits, a 0.056% hit rate.

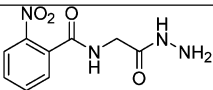
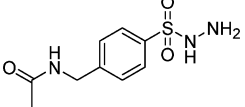
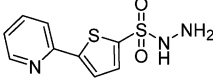
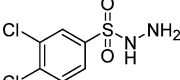
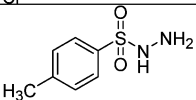
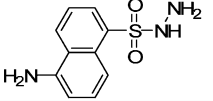
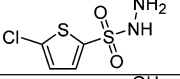
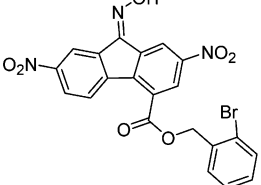
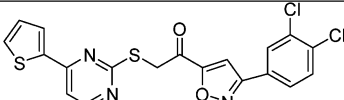
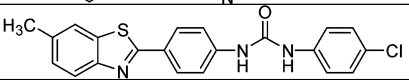
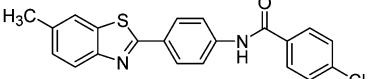
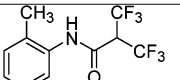
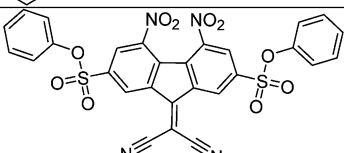
**Hit Analysis.** An  $IC_{50}$  analysis was performed on all 28 putative hit molecules from the primary screen. This identified 13 confirmed inhibitors of CBL with well-behaved  $IC_{50}$  curves (Table 1). We noted that eight of these showed changes in the visible spectra of CBL and free PLP (e.g., Figure 3). Seven of these (compounds 1–7) were hydrazides or sulfonylhydrazides, which are known to interact with the cofactor of PLP enzymes, and one, compound 8, was an oxime. We reasoned that the surprising interaction we observed with 8 was the result of hydrolysis of the oxime to generate hydroxylamine in situ that interacted with the PLP cofactor. The visible spectrum of CBL in the presence of  $NH_2OH$  was identical to that of 8 and CBL (not shown).

Compounds 9–13 did not alter the UV–vis spectrum of CBL. Rather, they behaved as typical reversible inhibitors with mixed inhibition (Table 2). This type of inhibition means that the



**Figure 2.** Results of the high-throughput screen of *E. coli* CBL vs 50 000 small molecules. The screen was performed in duplicate, and the results of each replicate of 50 000 are plotted against each other. The solid line indicates the hit cutoff, and 98.8% of the data are shown.

**Table 1.** Inhibitors of CBL Identified by High-Throughput Screening

Compound	Structure	IC <sub>50</sub> ( $\mu$ M)	Interaction with PLP
1		4.5 $\pm$ 0.6	Yes
2		34 $\pm$ 4	Yes
3		3.4 $\pm$ 0.9	Yes
4		1.8 $\pm$ 1.2	Yes
5		2.2 $\pm$ 0.1	Yes
6		6 $\pm$ 1	Yes
7		6.9 $\pm$ 0.6	Yes
8		0.53 $\pm$ 0.04	Yes
9		2.7 $\pm$ 0.1	No
10		16 $\pm$ 1	No
11		200 $\pm$ 150	No
12		0.28 $\pm$ 0.06	No
13		9 $\pm$ 1	No

compounds bind to both the free enzyme and the enzyme–substrate complex and are therefore not likely to bind to the active site.

**Structure of CBL in Complex with Compound 1.** CBL was cocrystallized with compound **1**, and the 3D structure of the complex was determined to 1.8 Å resolution (pdb code 2GQN) (Table 3, Figure 4A). The conditions used to obtain the inhibitor-bound CBL crystals were similar to those reported by Clausen et al.<sup>18</sup> for the determination of the PLP-bound enzyme. CBL exists as a tetramer in solution;<sup>19</sup> however, in the C222<sub>1</sub> crystal, a dimer was observed within the asymmetric

unit. The complete  $\alpha 4$  tetramer as shown in Figure 4A is assembled by combining two dimers related by a crystallographic 2-fold axis. Excellent detailed descriptions of the entire CBL structure from both *E. coli*<sup>18</sup> and *Arabidopsis*<sup>20</sup> have been reported; therefore, only a brief description is given here. Four equivalent active sites exist within the CBL tetramer. Each active site contains a single PLP cofactor molecule bound deep within a cleft formed between equivalent dimer interfaces (Figure 4A). Thus, residues from two monomers orchestrate substrate binding and catalysis at a given active site. In the absence of substrate, PLP remains covalently bound to lysine-210 via a Schiff base<sup>18</sup> (Figure 4B). Currently, no crystal structures are currently

<sup>a</sup> Abbreviations: CBL, cystathionine  $\beta$ -lyase; PLP, pyridoxal phosphate.

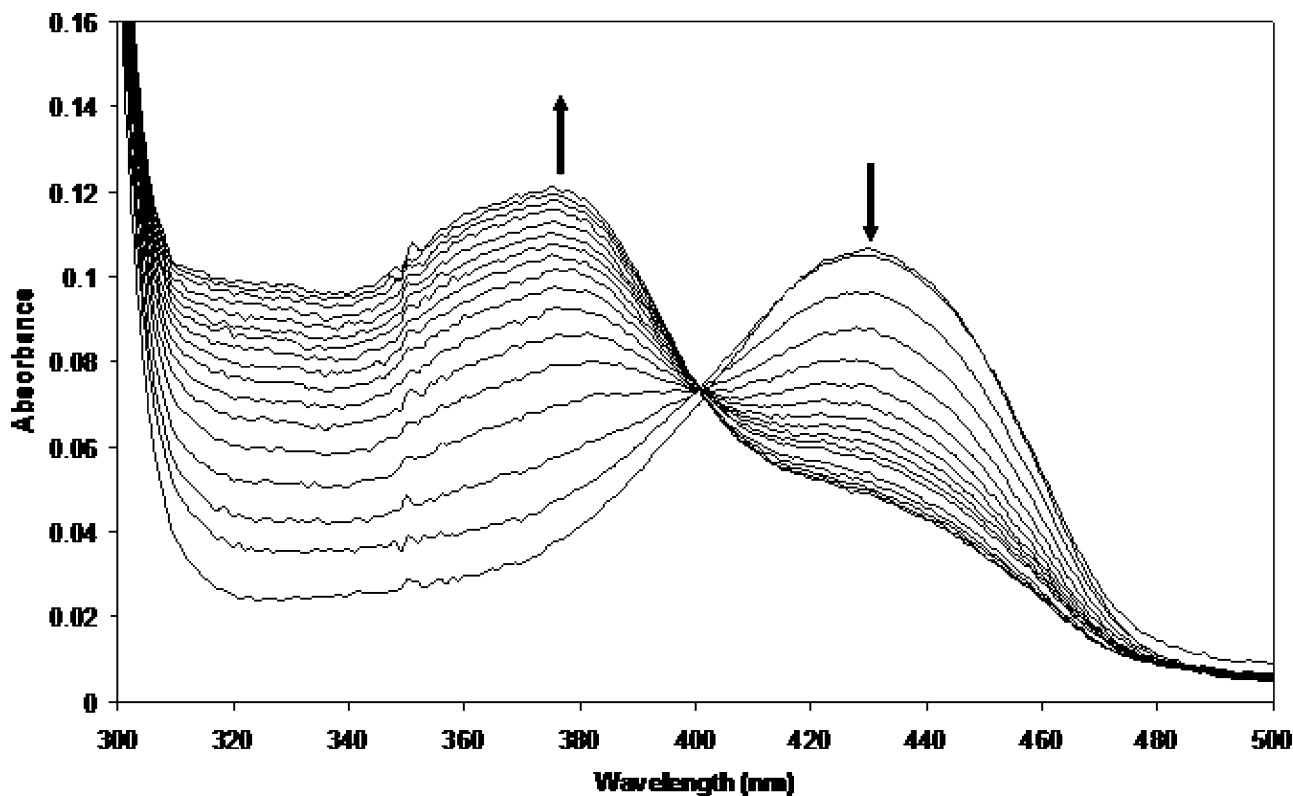


**Figure 3.** Representative titration of CBL by PLP-interacting compounds. UV-vis spectra were recorded every 1 to 2 min from 0 to 20 min following addition of 25  $\mu\text{M}$  **5** to 20 mM purified CBL. Arrows indicate the decrease in the characteristic PLP absorbance at 430 nm, whereas a new peak corresponding to the covalent adduct between the cofactor and the compound appears at 380 nm.

**Table 2.** Kinetic Parameters of Reversible Nonslow-Binding Inhibitors of CBL

compound	steady-state inhibition		
	type	$K_{is}$ ( $\mu\text{M}$ )	$K_{ii}$ ( $\mu\text{M}$ )
<b>8</b>	M	$0.13 \pm 0.02$	$0.28 \pm 0.03$
<b>9</b>	M	$17.7 \pm 0.2$	$10.8 \pm 0.1$
<b>10</b>	NC	$28.7 \pm 0.3$	$28.7 \pm 0.3$
<b>11</b>	M	$800 \pm 600$	$1400 \pm 800$
<b>12</b>	M	$0.8 \pm 0.3$	$0.9 \pm 0.3$
<b>13</b>	M	$3 \pm 1$	$5 \pm 1$

available for CBL in the presence of either substrate or product; therefore, it is difficult to comment on the possibility of significant domain movements that may take place during the course of the reaction. The fact that significant differences in the C $\alpha$  positions of CBL were not observed (rmsd = 0.3  $\text{\AA}$ ) between inhibitor-bound (pdb 2GQN) and -unbound structures (pdb 1CL1) suggests that large domain movements may not be required during the course of the reaction.

Crystals grown in the absence of **1** were yellow because of the presence of bound PLP. However, when soaked in a solution containing 1 mM **1** these crystals became clear within 10–15 min. This color change is consistent with the spectral shift observed upon hydrazide formation when **1** reacts with bound PLP in CBL. The crystal structure confirmed the expected covalent complex between **1** and PLP. The observed C=N bond joining PLP and **1** is well ordered in the final model and has an average  $B$  value of 15.7  $\text{\AA}^2$  and a reasonable bond length of 1.28  $\text{\AA}$ . Examination of the structure revealed that the 2-nitrobenzamide moiety of **1** was located in a hydrophobic pocket of the protein flanked by Tyr56, Tyr238, Tyr338, and Phe55 (Figure 5A). No direct hydrogen bonding was observed between CBL and the 2-nitrobenzamide group. The active sites of both monomers within the asymmetric unit were fully occupied by

**Table 3.** Crystallographic Data and Refinement Statistics of CBL in Complex with **1** and **18**

data set	Data Collection	
	<b>1</b>	<b>18</b>
Space group	C2221	C2221
Unit-cell parameters ( $\text{\AA}$ )	$a = 59.6$ $b = 153.0$ $c = 151.2$ $\alpha = \beta = \gamma = 90$	$a = 59.8$ $b = 153.5$ $c = 151.5$ $\alpha = \beta = \gamma = 90$
No. of molecules in asymmetric unit	2	2
Resolution range ( $\text{\AA}$ ) <sup>a</sup>	76.47–1.80 (1.86–1.80)	76.70–1.75 (1.81–1.75)
Unique reflections	64 262	70 456
Data Redundancy <sup>a</sup>	6.77 (6.13)	4.87 (4.19)
Completeness (%) <sup>a</sup>	99.7 (98.2)	99.8 (99.7)
$I/\sigma$ (I) <sup>a</sup>	11.4 (5.2)	10.7 (3.8)
$R_{\text{merge}}$ (%) <sup>a</sup>	7.8 (30.3)	8.0 (30.8)
Model and Refinement		
Resolution range ( $\text{\AA}$ ) <sup>a</sup>	76.47 – 1.80	76.70 – 1.78
$R_{\text{work}}$ (%)	17.3	16.6
$R_{\text{free}}$ (%)	22.2	22.1
No. of reflections	60,975	63,627
No. of amino acid residues/atoms	781/6031	781/6031
No. of waters	1264	1190
r.m.s.d bond lengths ( $\text{\AA}$ )	0.021	0.016
r.m.s.d bond angles ( $^\circ$ )	1.956	1.66
Average $B$ factor ( $\text{\AA}^2$ )	25.51	23.85

<sup>a</sup> Data for the highest-resolution shell are shown in parentheses.

**1** covalently bound to PLP. The average  $B$  factors of the atoms within the **1**–PLP complex and the CBL atoms within 3.5  $\text{\AA}$  of this complex are quite similar at 16.5 and 19.1  $\text{\AA}^2$ , respectively.

A comparison of the **1**-bound structure of CBL with that of the previously determined PLP-bound structure (pdb 1CL1)

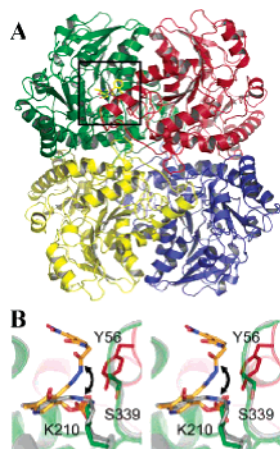


**Figure 4.** Structure of the CBL tetramer. (A) Ribbon diagram illustrating CBL quaternary structure. Monomers A (blue) and B (green) form the dimer observed within the asymmetric unit. This dimer is related to the A' (yellow) B' (red) dimer by a crystallographic 2-fold axis, which in turn completes the biologically active tetramer. One of four active sites within the tetramer is indicated by a black box. (B) Stereoview of the active-site region of CBL. Ribbon diagram illustrating the superimposition of PLP-bound CBL in the absence (gray ribbon and stick; pdb code 1CL1) and presence of **1** (green ribbon and stick). The **1**-PLP complex is shown by the yellow sticks. The black arrow highlights the alteration in PLP orientation upon inhibitor binding.

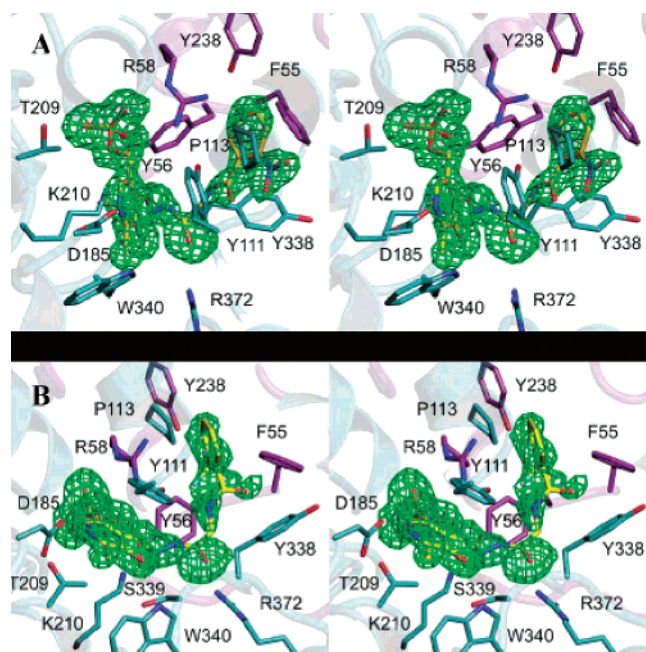


**Figure 5.** Structures of CBL bound to (A) **1** and (B) **18**. Stereoviews of the active-site region of CBL are shown in which PLP (yellow) is covalently bound to the inhibitor. Amino acid residues contributed from monomers B and B' are cyan and purple, respectively. PLP-inhibitor omit maps ( $F_o - F_c$ ,  $\sigma$  2.5) are shown in green mesh.

revealed only minor changes in the overall geometry and position of the amino acid side chains within the active site region. The most significant changes involved Lys210 and PLP (Figures 4B and 5A). Upon covalent bond formation with **1**, PLP was released from its covalent interaction with Lys210. This resulted not only in a  $35^\circ$  rotation of PLP about the plane of the pyridoxal ring but also in a reorientation of the Lys210 side chain, bringing it into hydrogen-bonding distance of both Ser339 and Tyr56 (2.7 and 3.0 Å, respectively).

Even in the presence of **1**, the deep substrate-binding cleft of CBL was not fully occupied. At least 15 ordered water

**Table 4.** Inhibition of CBL by a Library of Analogues of Compound **1**

Compound	Structure	IC <sub>50</sub> (μM)
14		25 ± 4
15		5.9 ± 0.6
16		82 ± 3
17		60 ± 20
18		0.079 ± 0.02
19		37 ± 3
20		15 ± 3
21		0.65 ± 0.03
22		560 ± 70
23		500 ± 100

molecules were located in the substrate-binding cleft. In principle, several of these water molecules could be replaced by modifications made to **1**. Thus, there is considerable potential to improve upon the affinity and certainly the specificity of **1**-CBL interactions.

**Synthesis of Derivatives of Compound 1.** We reasoned that a focused library of derivatives of **1** that retained the reactive acetic hydrazide group but varied the benzamide function to explore possible additional binding in the hydrophobic pocket could improve binding affinity. We therefore prepared **14**–**23** and measured their interaction with purified CBL (Table 4). Naphthyl substituents (**22** and **23**) were poor inhibitors of the enzyme, whereas most benzamide derivatives were comparable to **1**. The 2,3,5-trifluoro-4-methoxy-benzamide (**21**) and the 2-trifluoromethyl derivative (**18**) showed nanomolar IC<sub>50</sub>'s and retained PLP binding activity. Therefore, we next determined the 3D structure of **18** in complex with CBL.

A comparison of the 3D structures of **1** and **18** in complex with CBL revealed a number of similarities (Figure 5). As expected, both compounds occupied the same general space within the complexes, burying essentially identical surface areas (difference = 33 Å<sup>2</sup>). The anchoring effect of PLP in combination with the relatively short tether greatly limited the possibility of any dramatic alterations. Compound **18** underwent a  $180^\circ$

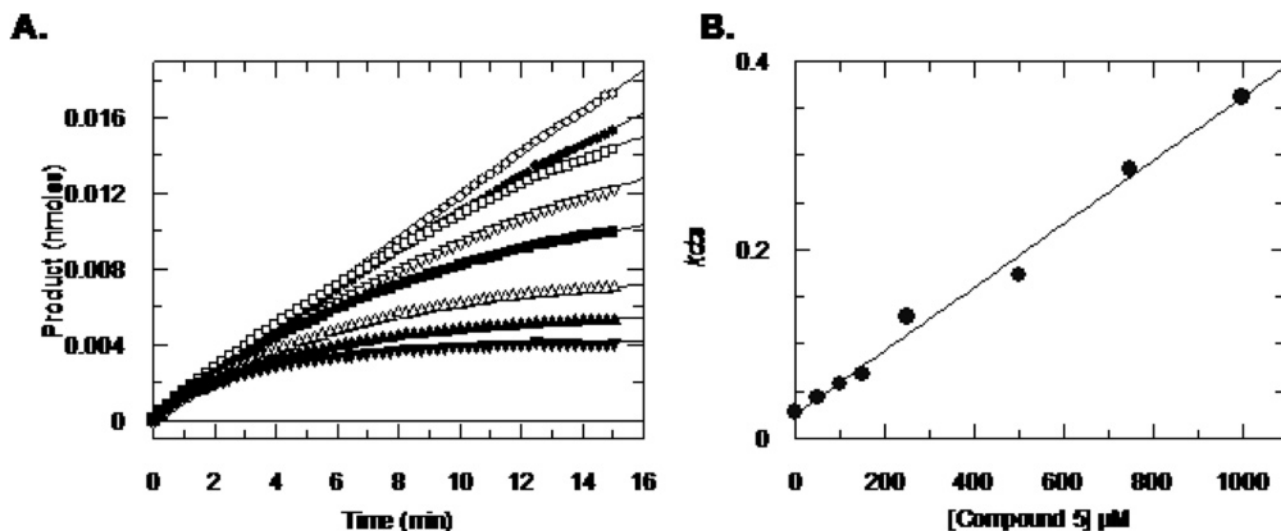
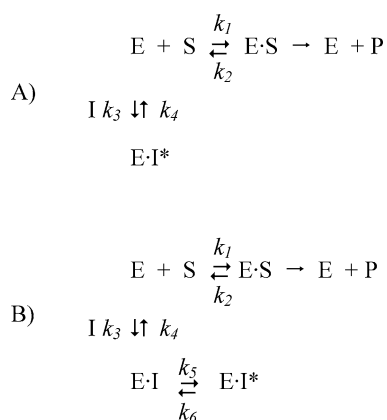


**Figure 6.** Slow-binding inhibition of CBL by **5**. (A) Progress curves showing the slow onset of inhibition by **5**: 0 (○), 50 (●), 100 (□), 150 (▽), 250 (■), 500 (△), 750 (▲), and 1000 μM. (B) Replot of  $k_{\text{obs}}$  vs concentration of **5**. Values for  $k_{\text{obs}}$  were determined by fitting evaluation 2 to the data in Figure 6A.

rotation of the benzene moiety that positioned the electronegative trifluoromethyl group away from the solvent and into contact with Tyr238 and Arg58. In addition, Tyr111 made a new hydrogen bond contact with the N4 atom of **18**. Thus, compared to **1**, **18** makes three additional hydrogen bonds with CBL without the loss of van der Waals contacts. These changes reflect the observed differences in the  $\text{IC}_{50}$  measurements for **1** and **18**. Because the binding of **18** leaves 15 or more water molecules in the substrate-binding cleft of CBL, one would expect increased affinity and specificity for CBL by further modifications to **18** if these could displace the ordered waters.

**Characterization of Slow-Binding Inhibition.** Compounds **1–7** and **14–23** bind to the PLP cofactor of CBL as assessed by UV–vis absorption spectra (e.g., Figure 3). Such interactions are frequently suggestive of slow-binding inhibition.<sup>21–23</sup> Slow-binding phenomena can be classified into two general mechanisms: one in which the slow formation of the stable enzyme–inhibitor complex (EI\*) occurs without kinetic accumulation of the EI inhibitor–enzyme collision complex (mechanism A) and one where it does (mechanism B):



We first examined the slow-binding behavior of **5** because it was readily available and showed good inhibition. The progress curves for the generation of homocysteine were consistent with slow the development of an  $\text{EI} \rightleftharpoons \text{EI}^*$  equilibrium (Figure 6A).<sup>23</sup> The progress curves were next fit to eq 2 to provide a measure of  $k_{\text{obs}}$ , the first-order rate constant for the formation of  $\text{EI}^*$  and replotted as a function of the inhibitor concentration (Figure

6B). This plot did not show saturation kinetics but gave a straight line. Such a relationship is consistent with mechanism A. From this steady-state analysis,  $k_3$  was determined to be  $0.34 \text{ nM}^{-1} \text{ min}^{-1}$ ,  $k_4$  was  $0.026 \text{ min}^{-1}$ , and the dissociation constant  $K_1^*$  was  $76 \text{ μM}$ .

Attempts to determine the steady-state slow-binding characteristics of **18** using this approach were problematic because of the rapid formation of the  $\text{ESI}^*$  complex. We therefore used a stopped-flow approach to measure the formation of the covalent complex directly by monitoring the decrease in absorbance at 430 nm.<sup>21</sup> Using **5**, a plot of  $k_{\text{obs}}$  versus [inhibitor] gave a straight line with a  $k_4$  (y intercept) of  $0.002 \text{ s}^{-1}$  and a  $k_3$  (slope) of  $0.08 \text{ nM}^{-1} \text{ s}^{-1}$ .  $K_1^*$  was estimated from  $k_4/k_3$  to be  $30 \text{ μM}$ . Using **18**, we obtained a  $k_4$  of  $0.033 \text{ s}^{-1}$ , a  $k_3$  of  $5 \text{ nM}^{-1} \text{ s}^{-1}$ , and a  $K_1^*$  of  $6.2 \text{ μM}$ .

The differences between the kinetic constants measured by steady state and stopped flow for **5** could be the result of the differences in the assay pH used in the two studies. It does suggest that mechanism A is likely not adequate in explaining the interactions of the molecules with CBL and that there is likely a contribution of a low-affinity collision complex to the process such that mechanism B is a more reasonable model despite the lack of saturation in the  $k_{\text{obs}}$  versus [inhibitor] plot. Such differences have been noted previously for slow-binding inhibitors of CBL<sup>21</sup> and have been similarly rationalized. In such a case, the  $K_1$  describing the formation of the EI complex is much larger than the  $K_1^*$  and the range of inhibitor concentrations sampled in the experiment, thereby explaining the absence of saturation kinetics. Despite these discrepancies, the overall trend that **18** is a much more effective inhibitor of CBL than **5** as determined by  $\text{IC}_{50}$  determination is supported by the stopped-flow analysis.

The inhibition by these compounds was slowly reversible (e.g., the regained activity of CBL inhibited by **5** was 13% over 2 h). This is consistent with the crystal structures of **1** and **5** in complex with the enzyme in which there is no additional covalent interaction except with the PLP cofactor.

**Antimicrobial Activity.** A selection of the hit compounds identified in the screen was examined for antimicrobial activity against the pathogenic yeast, *Candida albicans* and against *E. coli* (Table 5). Several of the hydrazine compounds and **8** showed modest activity against *E. coli*, whereas only **12**

**Table 5.** MIC Values for Selected CBL Inhibitors

compound	MIC ( $\mu\text{g/mL}$ )		
	<i>Candida albicans</i> ATCC no. 90028	<i>E. coli</i>	
		ATCC no. 25922, + methionine	ATCC no. 25922, - methionine
1	128	16	16
2	>128	64	64
3	>128	32	32
5	128	64	32
8	>128	64	64
9	>128	>128	>128
10	>128	>128	>128
11	>128	>128	>128
12	16	64	32
14	>128	64	32
15	>128	128	128
16	>128	128	128
17	>128	>128	>128
18	>128	>128	>128
19	>128	>128	>128
20	>128	128	128
21	>128	>128	>128
22	>128	>128	>128

exhibited antifungal activity against *C. albicans* in the presence and absence of methionine. Antimicrobial activity did not correlate with CBL  $\text{IC}_{50}$ 's.

**Summary and Conclusions.** A high-throughput screening of bacterial CBL has identified reversible and slow-binding inhibitors of the enzyme, some with antimicrobial activity. Analysis of the X-ray structure of the complex of CBL with **1** confirmed the expected formation of the PLP adduct and established the synthesis of a small library of analogues. One of these, **18**, exhibited a 50-fold improved inhibition of CBL. This was a surprising result because **1** and **18** differ only by the substitution of a trifluoromethyl group in **18** for the nitro group at position 2 of the benzamide ring in **1**. The 3D structure of the complex of **18** with CBL revealed that this small change resulted in an  $\sim 180^\circ$  rotation of the benzamide ring in the CBL active site, facilitating the formation of a new H-bond between Tyr111 and **18**. Additional analogues of **18** that take advantage of this H-bonding opportunity could have improved activity. These results demonstrate that improved inhibitors of CBL can be discovered with a combination of 3D complex determination and library synthesis. Unfortunately, CBL inhibition did not correlate well with antimicrobial activity. There could be myriad reasons for this, including transport into the cell, efflux, and metabolism. Future work will require an understanding of this discrepancy. Although we have shown that antimicrobial activity did not track well with CBL affinity in this study, the fact that CBL is important to virulence and methionine biosynthesis and is tractable in high-throughput screening and structure-based drug design demonstrates that this enzyme has significant potential as a new antimicrobial target. When set on a backdrop of increasing antibiotic resistance and a paucity of new agents and targets, this research provides encouragement that amino acid biosynthetic pathways are worthy of exploration in antibiotic development.

## Experimental Procedures

**Materials.** *E. coli* CBL<sup>12</sup> and VanHst<sup>24</sup> were purified as previously described. The small-molecule library was purchased from Maybridge Plc. (Cornwall, England) and is composed of high-quality small druglike molecules of an average molecular mass of 325 g/mol.

**High-Throughput Screen of *E. coli* CBL.** Enzyme activity was measured by titration of the formation of homocysteine at 412 nm using 5,5'-dithio-bis-(2-nitrobenzoic acid). The screen was per-

formed on a Beckman/Coulter-SAGIAN core automated system (Beckman/Coulter Inc., Fullerton, CA) at the McMaster High Throughput Screening Laboratory in 96-well polystyrene plates. Each well contained 3.25 mM 5,5'-dithio-bis-(2-nitrobenzoic acid) (DTNB) and 24 nM CBL in 50 mM TAPS at pH 8.5. Library compounds dissolved in DMSO were added to a concentration of  $\sim 10 \mu\text{M}$  (based on an average molecular mass of 325 g/mol), and the mixture was incubated at room temperature for 10 min. Substrate cystathionine (CTT) was then added to 100  $\mu\text{M}$ , and the reaction was monitored continuously for 4 min using a SpectraMax plate reader (Molecular Devices Corp., Sunnyvale, CA). The final volume was 100  $\mu\text{L}$ , and the final concentration of DMSO was 5%, which does not affect CBL activity. High controls (100% enzyme activity) contained only DMSO, and low controls (0% enzyme activity) lacked CBL; each compound in the library was tested in duplicate. Enzyme activity was calculated in ActivityBase (IDBS) from the slope of the data between 30 and 200 s. The residual activity was calculated as [(sample data - mean of low controls)/(mean of high controls - mean of low controls)]  $\times$  100. A statistical analysis of the screen was performed using the Z and Z' parameters.<sup>17</sup>

**Hit Analysis.** Compounds were considered hits if the residual activity of CBL was below 20% for both replicate measurements. Outliers (where one replicate was a potential hit and the other was not) were rescreened in duplicate. The  $\text{IC}_{50}$ 's of the hit compounds were determined in triplicate using 12 concentrations of the compound under the conditions used in the primary screen except for the concentration of 5,5'-dithio-bis-(2-nitrobenzoic acid) maintained at 1 mM. Kinetic data were fit to eq 1 using the program Grafit 4<sup>25</sup> where  $D$  = minimum response plateau,  $A$  = maximum response plateau,  $I$  = concentration of inhibitor, and  $S$  = slope factor.

$$y = \frac{A - D}{1 + \left(\frac{I}{\text{IC}_{50}}\right)^S} + D \quad (1)$$

Hit molecules that showed good  $\text{IC}_{50}$  behavior (well-defined plateaus, slope factor close to 1) and that were not titrating the PLP cofactor were further analyzed with a full  $K_i$  determination in triplicate using a range of CTT concentrations from 25 to 600  $\mu\text{M}$ .

For compounds containing groups that react with DTNB, a confirmatory assay was developed that coupled pyruvate generation with NADH reduction by VanHst.<sup>24</sup> Each assay contained 24 nM CBL, inhibitor in DMSO, 100  $\mu\text{M}$  CTT, 100  $\mu\text{M}$  NADH, 60  $\mu\text{g/mL}$  VanHst, and 50 mM TAPS at pH 8.5. The assays were monitored at 340 nm. The reversibility of the inhibition was confirmed by dilution and overnight dialysis. The interaction of the compounds with the PLP cofactor of CBL was assessed by measuring the absorbance spectrum between 300 and 500 nm on a Cary 300 spectrophotometer. These studies were performed using 20  $\mu\text{M}$  purified CBL in 25 mM HEPES at pH 7.5 in a total volume of 0.8 mL.

Slow-binding studies were carried out by monitoring the activity of CBL over time in an assay mixture containing 12 nM CBL, 5% DMSO, 1500  $\mu\text{M}$  CTT, 3 mM DTNB, 50 mM TAPS at pH 8.5, and 0 to 1000  $\mu\text{M}$  inhibitor. The reactions were monitored at 412 nm using a SpectraMax Plate Reader (Molecular Devices Corp., Sunnyvale, CA).

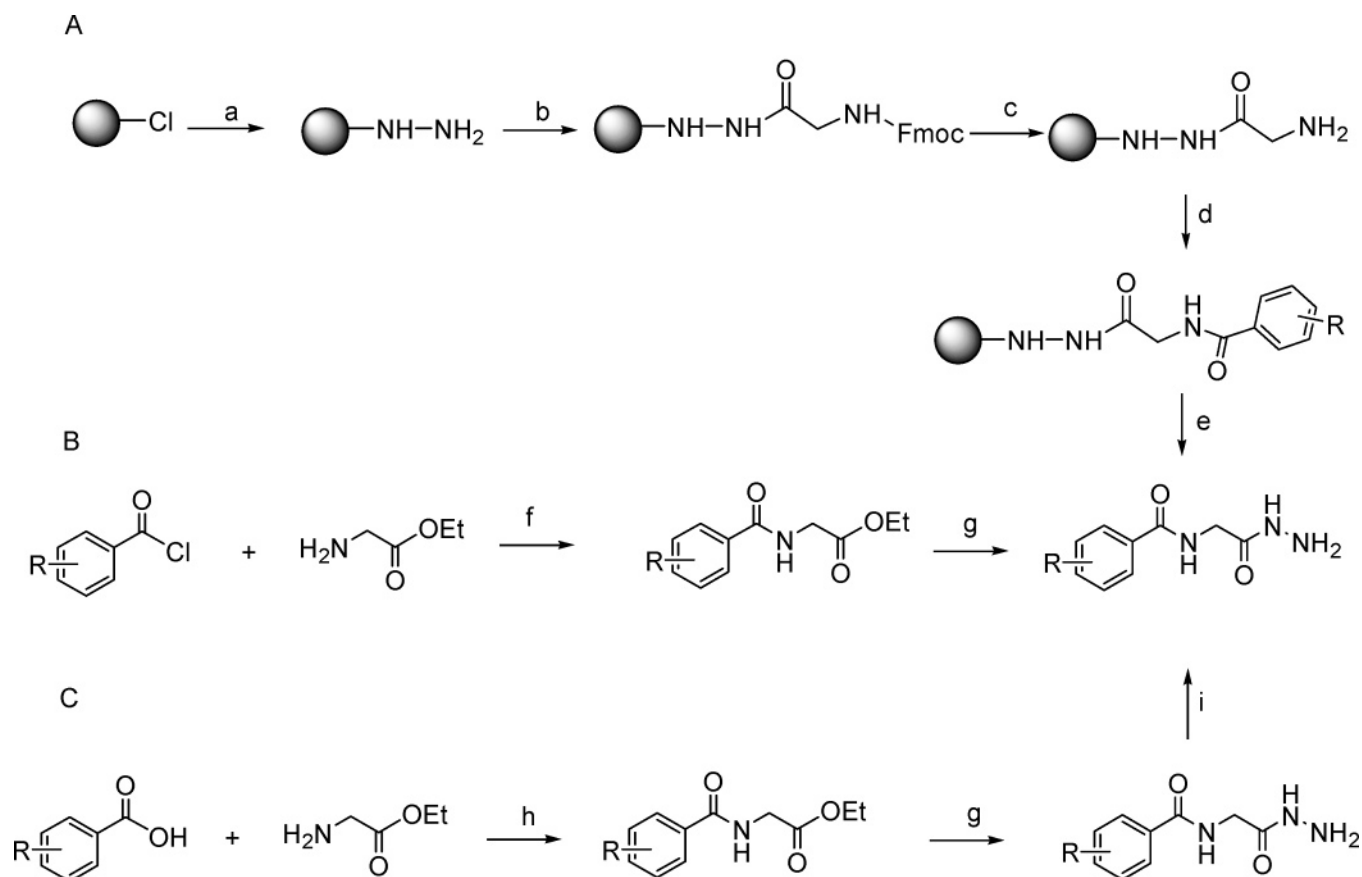
The data were fit to eq 2

$$P = v_s t + (v_0 - v_s)[1 - \exp(-k_{\text{obs}} t)]/k_{\text{obs}} \quad (2)$$

where  $P$  = product formed,  $v_0$  = initial velocity,  $v_s$  = steady-state velocity,  $t$  = time, and  $k_{\text{obs}}$  is the rate constant for the formation of the inhibited complex ( $\text{EI}^*$ ) from the initial collision complex  $\text{EI}$ .<sup>23</sup> The individual rate and inhibition constants were determined from a replot of  $k_{\text{obs}}$  versus [inhibitor].

Slow-binding studies were also conducted using a stopped-flow apparatus. Rapid mixing was achieved using a BioLogic stopped flow SFM-400 mixer and an MPS-50 controller (Molecular Kinetics, Seattle, WA). The reaction was monitored at 430 nm using

Scheme 2



a MOS-250 fast reaction spectrophotometer with an FC cuvette, path length 2 mM. Data acquisition was with Bio-Kine software. For **5**, the assay contained 12.7  $\mu\text{M}$  CBL, 0 to 0.5% DMSO, 0 to 1250  $\mu\text{M}$  compound, and 25 mM HEPES at pH 7.5. For **18**, the assay contained 19.8  $\mu\text{M}$  CBL, 0 to 1% DMSO, 0 to 300  $\mu\text{M}$  compound, and 25 mM HEPES at pH 7.5.

The data were fit to eq 3

$$A = A_S + (A_0 - A_S)\exp(-k_{\text{obs}}t) \quad (3)$$

where  $t$  is time,  $A_0$  and  $A$  are the absorbances at time zero and time  $t$ , respectively, and  $A_S$  is the final steady-state absorbance. The individual rate and inhibition constants were determined from replots of  $k_{\text{obs}}$  versus [inhibitor].

**Synthesis of Inhibitors.** All benzoic acids and acid chlorides were from Sigma-Aldrich Canada Ltd. (Oakville, ON, Canada). Hydrazine (anhydrous) was from J. T. Baker Chemicals Co. (Phillipsburg, N.J.). 2-Chlorotrityl resin, Fmoc-glycine, and *N*-hydroxybenzotriazole (HOBt) were from Novabiochem (San Diego, CA). Glycine ethyl ester hydrochloride was from Sigma (St. Louis, MO). 3,5-*N*-Di-*t*-butyl-protected benzoic acid and 2-*N*-*t*-butyl-protected naphthoic acid were synthesized using standard procedures.<sup>26</sup> Purity of the compounds was monitored by analytical reversed-phase HPLC (Acclaim TM<sup>120</sup> column, 3  $\mu\text{m}$  120 Å, 4.6  $\times$  150 mm<sup>2</sup>) using water–acetonitrile gradients with 0.05% trifluoroacetic acid (TFA) as a counterion. The identity of all products was verified by liquid chromatography electrospray mass spectrometry (LC/ES-MS) analysis performed on QTRAP-LC/MS/MS (Applied Biosystems). High-resolution mass spectra (HRMS) were obtained on a high-resonance electrospray time-of-flight mass spectrophotometer (TOFMS ES<sup>+</sup>). <sup>1</sup>H and <sup>13</sup>C NMR were recorded on a Bruker AV 200 NMR spectrometer, and chemical shifts are reported in parts per million relative to tetramethylsilane as an internal standard. The data are reported as follows: chemical shift, multiplicity (s = singlet, d = doublet, t = triplet, m = multiplet), integration, and coupling constant (Hz).

Two different approaches were taken to synthesize analogues of hit molecules: first, compounds were synthesized on a solid support (method A), and then the most successful ones were scaled up using solution-phase synthesis (method B or C) (Scheme 2).

**Solid-Phase Synthesis (Method A).** The 2-chlorotrityl resin was first derivatized with hydrazine (10 eq) followed by Fmoc-Gly-OH (10 equiv) activation and coupling using dicyclohexylcarbodiimide (DCC)/hydroxybenzotriazole (HOBt). Substitution was estimated to be 0.2 mmol/g resin. After Fmoc deprotection, the resin was divided and reacted with corresponding benzoic acid derivatives. Finally, hydrazides were cleaved from the resin with 10% TFA/dichloromethane for 2 h at room temperature. All products were purified using reversed-phase HPLC (C18).

**Solution-Phase Synthesis Employing Acid Chlorides (Method B).** This approach was modified from a literature method.<sup>27</sup> To a solution of glycine ethyl ester hydrochloride (0.66 g, 4.8 mmol) and triethylamine (0.53 g, 5.2 mmol) in 10 mL of diethyl ether was added a solution of corresponding benzoyl chloride (4.8 mmol) in 10 mL of diethyl ether. The reaction was carried out for 4 h at room temperature. The precipitate formed was filtered out and dissolved in absolute ethanol (10 mL), and to this solution was added anhydrous hydrazine (0.5 mL). The reaction was carried out for 4 more hours. After solvent evaporation, the crude product was purified using reversed-phase HPLC.

**Solution-Phase Synthesis Employing Mixed Anhydrides (Method C).** *N*-*t*-Butyloxycarbonyl-protected acid (1.8 mmol) was coupled to glycine ethyl ester using the isobutylcarbonyl acid mixed anhydrides procedure as described before.<sup>26</sup> The dry residue was dissolved in 5 mL of ethanol, and 0.5 mL of hydrazine was added to this solution. The reaction was carried out for 4 h at room temperature and then concentrated under reduced pressure, suspended in 5 mL 50/50 acetonitrile/water, and lyophilized. The crude, dry product was subjected to Boc deprotection in a solution of dichloromethane (5 mL), TFA (2.5 mL), triisopropylsilane (0.2 mL), and water (0.2 mL) for 1 h at room temperature. After solvent

removal, the final product was precipitated with cold ether and further purified using reversed-phase HPLC.

**N-Hydrazinocarbonylmethyl-4-nitrobenzamide (14, Method B).** Yield of 23% over two steps. ES-MS ( $C_9H_{10}N_4O_4$  MW 238.20): (ES<sup>+</sup>) 239.0 [M + H]<sup>+</sup>, (ES<sup>-</sup>) 237.0 [M - H]<sup>-</sup>. <sup>1</sup>H NMR ( $d_6$ -DMSO): 8.13 (m, 2H, Ar); 8.06 (m, 2H, Ar); 3.70 (s, 2H, CH<sub>2</sub>). <sup>13</sup>C NMR ( $d_6$ -DMSO): 177.26, 173.45, 136.28, 135.21, 134.10, 130.70, 47.89.

**N-Hydrazinocarbonylmethyl-3,5-dinitrobenzamide (15, Method B).** Yield of 31% over two steps. ES-MS ( $C_9H_9N_5O_6$  MW 283.20): (ES<sup>+</sup>) 284.0 [M + H]<sup>+</sup>, (ES<sup>-</sup>) 282.2 [M - H]<sup>-</sup>. <sup>1</sup>H NMR ( $d_6$ -DMSO): 9.06 (s, 1H, Ar); 8.97 (s, 2H, Ar); 4.32 (s, 2H, CH<sub>2</sub>). <sup>13</sup>C NMR ( $d_6$ -DMSO): 176.20, 170.20, 155.52, 134.83, 128.26, 124.41, 48.01.

**3,5-Diamino-N-hydrazinocarbonylmethyl-benzamide (16, Method C).** Yield of 12% over four steps. ES-MS ( $C_9H_{13}N_5O_2$  MW 223.23): (ES<sup>+</sup>) 224.2 [M + H]<sup>+</sup>; (ES<sup>-</sup>) 222.2 [M - H]<sup>-</sup>. <sup>1</sup>H NMR (D<sub>2</sub>O): 7.47 (s, 2H, Ar); 7.24 (s, 1H, Ar); 3.79 (s, 2H, CH<sub>2</sub>). <sup>13</sup>C NMR (D<sub>2</sub>O): 174.08, 169.47, 142.87, 139.29, 128.83, 127.89, 47.89.

**N-Hydrazinocarbonylmethyl-2,6-dimethoxybenzamide (17, Method B).** Yield of 28% over two steps. ES-MS ( $C_{11}H_{15}N_3O_4$  MW 253.25): (ES<sup>+</sup>) 254.2 [M + H]<sup>+</sup>; (ES<sup>-</sup>) 252.1 [M - H]<sup>-</sup>. <sup>1</sup>H NMR (D<sub>2</sub>O): 7.28 (m, 1H, Ar); 6.61 (d, 2H, J 8.5, Ar); 3.68 (s, 6H, CH<sub>3</sub>); 3.66 (s, 2H, CH<sub>2</sub>). <sup>13</sup>C NMR (D<sub>2</sub>O): 165.80, 163.54, 161.20, 139.92, 138.94, 111.46, 62.82, 49.31.

**N-Hydrazinocarbonylmethyl-2-trifluoromethylbenzamide (18, Method B).** Yield of 20% over two steps. ES-MS ( $C_{10}H_{10}F_3N_3O_2$  MW 261.20): (ES<sup>+</sup>) 262.1 [M + H]<sup>+</sup>; (ES<sup>-</sup>) 260.0 [M - H]<sup>-</sup>. <sup>1</sup>H NMR (D<sub>2</sub>O-*d*<sub>3</sub>-acetonitrile = 1:1): 7.68 (d, 1H, J 6.8, Ar); 7.48 (m, 3H, Ar); 3.91 (s, 2H, CH<sub>2</sub>).

<sup>13</sup>C NMR (D<sub>2</sub>O-*d*<sub>3</sub>-acetonitrile = 1:1): 176.68, 173.92, 149.10, 139.52, 137.69, 135.35, 133.52, 127.51, 125.99, 46.46.

**N-Hydrazinocarbonylmethyl-3-trifluoromethylbenzamide (19, Method B).** Yield of 15% over two steps. ES-MS ( $C_{10}H_{10}F_3N_3O_2$  MW 261.20): (ES<sup>+</sup>) 262.1 [M + H]<sup>+</sup>; (ES<sup>-</sup>) 260.0 [M - H]<sup>-</sup>. <sup>1</sup>H NMR ( $d_6$ -DMSO): 9.07 (s, 1H, NH); 8.21 (s, 1H, Ar); 8.17 (d, 2H, J 7.5 Hz, Ar); 7.90 (d, 1H, J 7.4 Hz, Ar); 7.69 (t, 1H, J<sub>1</sub> 7.7 Hz, J<sub>2</sub> 7.6 Hz, Ar); 3.87 (d, 2H, J 5.7 Hz, CH<sub>2</sub>). <sup>13</sup>C NMR ( $d_6$ -DMSO): 175.46, 172.43, 142.13, 138.80, 136.89, 135.25, 131.35, 125.91, 48.73.

**N-Hydrazinocarbonylmethyl-4-trifluoromethylbenzamide (20, Method B).** Yield of 16% over two steps. ES-MS ( $C_{10}H_{10}F_3N_3O_2$  MW 261.20): (ES<sup>+</sup>) 262.1 [M + H]<sup>+</sup>; (ES<sup>-</sup>) 260.0 [M - H]<sup>-</sup>. <sup>1</sup>H NMR ( $d_6$ -DMSO): 9.33 (s, 1H, NH); 8.05 (d, 2H, J 5.7 Hz, Ar); 7.84 (d, 1H, J 8.4 Hz, Ar); 3.85 (d, 2H, J 5.7 Hz, CH<sub>2</sub>). <sup>13</sup>C NMR ( $d_6$ -DMSO): 174.26, 170.41, 137.57, 136.81, 135.25, 131.35, 48.81.

**2,4,5-Trifluoro-N-hydrazinocarbonylmethyl-3-methoxybenzamide (21, Method B).** Yield of 31% over two steps. ES-MS ( $C_{10}H_{10}F_3N_3O_3$  MW 277.07): (ES<sup>+</sup>) 278.2 [M + H]<sup>+</sup>. <sup>1</sup>H NMR ( $d_6$ -DMSO): 7.48 (s, 1H, Ar); 3.96 (s, 2H, CH<sub>2</sub>); 3.07 (s, 3H, OCH<sub>3</sub>). <sup>13</sup>C NMR ( $d_6$ -DMSO): 175.03, 169.25, 166.47, 165.83, 127.30, 121.36, 117.90, 117.10, 69.51, 52.77.

**2-Amino-naphthalene-1-carboxylic Acid Hydrazinocarbonylmethyl Amide (22, Method C).** Yield of 10% over four steps. ES-MS ( $C_{13}H_{14}N_4O_2$  MW 258.28): (ES<sup>+</sup>) 259.2 [M + H]<sup>+</sup>. <sup>1</sup>H NMR (D<sub>2</sub>O): 8.10 (s, 2H, Ar); 7.72 (m, 4H, Ar); 7.45 (m, 3H, Ar); 4.10 (s, 2H, CH<sub>2</sub>).

<sup>13</sup>C NMR (D<sub>2</sub>O): 176.34, 173.92, 140.43, 138.01, 137.25, 136.45, 135.51, 134.97, 134.18, 132.67, 130.28, 129.73, 47.73, 2.77, 15.67.

**N-Hydrazinocarbonylmethyl-2-naphthalen-1-yl-acetamide (23, Method C).** Yield of 25% over 2 steps. ES-MS ( $C_{14}H_{15}N_3O_2$  MW 257.27): (ES<sup>+</sup>) 258.2 [M + H]<sup>+</sup>.

<sup>1</sup>H NMR (D<sub>2</sub>O): 8.10 (s, 2H, Ar); 7.72 (m, 4H, Ar); 7.47 (m, 3H, Ar); 4.10 (s, 2H, CH<sub>2</sub>).

<sup>13</sup>C NMR (D<sub>2</sub>O): 176.34, 140.43, 138.01, 137.25, 136.65, 135.52, 134.87, 134.18, 132.67, 130.28, 129.73, 78.87, 48.73, 47.73.

**Determination of Minimum Inhibitory Concentrations (MICs).** MICs of hit compounds were determined in duplicate over a test range of 0.25–128  $\mu$ g/mL by broth microdilution methods accord-

ing to the NCCLS guidelines for using both bacterial and fungal test organisms in M9 medium with and without added methionine and in synthetic complete medium without methionine, respectively.

**Crystallization and X-Ray Structure Determination of CBL-Inhibitor Complexes.** Crystals of CBL-inhibitor complexes were grown using the hanging-drop vapor diffusion method. The crystallization conditions were similar to those previously reported in Clausen et al.<sup>18</sup> Specifically, CBL was concentrated to 5 mg/mL in 5 mM HEPES (pH 7.5), and inhibitor was added to a final concentration of 1 mM. Large (0.6 mm  $\times$  0.6 mm  $\times$  0.2 mm) single crystals grew at room temperature within 1 week upon mixing 2  $\mu$ L of the protein solution, 2  $\mu$ L of the precipitant solution containing 100 mM HEPES (pH 7.3), 150 mM CaCl<sub>2</sub>, and 26% PEG400. To obtain the highest-quality diffraction data, the crystals were soaked sequentially in the following two cryoprotecting solutions for 14 h and 5 min, respectively: cryosolution I (100 mM HEPES (pH 7.3), 150 mM CaCl<sub>2</sub>, 30% PEG400, 8 mM inhibitor) and cryosolution II (100 mM HEPES (pH 7.3), 150 mM CaCl<sub>2</sub>, 30% PEG400, 16 mM inhibitor). The crystals were flash frozen by transferring them directly into a nitrogen cold stream (100 K).

A single X-ray diffraction data set was collected using an RAXIS4++ image plate detector and Cu K $\alpha$  radiation from an RU300 rotating anode (Rigaku MSC). The apparent focal-spot size was set to 0.3 mm  $\times$  0.3 mm. Reflection data were processed, scaled, and reduced using D\*trek<sup>28</sup> and truncated using CCP4 (Leslie, 1990). Because the CBL-inhibitor crystals grew in the same space group (C222<sub>1</sub>) and with the same unit cell parameters ( $a = 59.6$  Å,  $b = 153.0$  Å,  $c = 151.2$  Å) as native CBL (pdb code 1CL1), the native phases were used to solve the structure. Iterative cycles of refinement and model building were performed with the programs REFMAC<sup>29–32</sup> and Coot,<sup>33</sup> respectively. The final models each contain two monomers of CBL in the asymmetric unit, each bound to a single inhibitor molecule. Analysis of the Ramachandran plots for these models calculated by PROCHECK<sup>34</sup> indicated that in both cases 92.6% of the residues are in the most-favored regions with the remaining 7.4% located in the allowed regions. Crystallographic data and final refinement statistics can be found in Table 1. Figures illustrating the structure of CBL were generated using the PyMol Molecular Graphics System.<sup>35</sup>

**Acknowledgment.** This work was supported by the Canadian Bacterial Disease Network Centre of Excellence, the Ontario Research and Development Fund, and by Canada Research Chair awards to E.D.B. and G.D.W.

**Acknowledgment. This Section Tagged Supporting Information**

**Supporting Information Available:** Additional HPLC and HRMS data. This material is available free of charge via the Internet at <http://pubs.acs.org>.

## References

- Coates, A.; Hu, Y.; Bax, R.; Page, C. The future challenges facing the development of new antimicrobial drugs. *Nat. Rev. Drug Discovery* **2002**, *1*, 895–910.
- Nathan, C. Antibiotics at the crossroads. *Nature* **2004**, *431*, 899–902.
- Brown, E. D.; Wright, G. D. New targets and screening approaches in antimicrobial drug discovery. *Chem. Rev.* **2005**, *105*, 759–774.
- Fasman, G. D. *Handbook of Biochemistry and Molecular Biology*, 3rd ed.; CRC Press: Cleveland, OH, 1976; Vol. 1, p 328.
- Wei, Y.; Lee, J. M.; Richmond, C.; Blattner, F. R.; Rafalski, J. A.; LaRossa, R. A. High-density microarray-mediated gene expression profiling of *Escherichia coli*. *J. Bacteriol.* **2001**, *183*, 545–556.
- Becker, D.; Selbach, M.; Rollenhagen, C.; Ballmaier, M.; Meyer, T. F.; Mann, M.; Bumann, D. Robust *Salmonella* metabolism limits possibilities for new antimicrobials. *Nature* **2006**, *440*, 303–307.
- Kugler, M.; Loeffler, W.; Rapp, C.; Kern, A.; Jung, G. Rhizocticin A, an antifungal phosphono-oligopeptide of *Bacillus subtilis* ATCC 6633: biological properties. *Arch. Microbiol.* **1990**, *153*, 276–281.

- (8) Aoki, Y.; Kondoh, M.; Nakamura, M.; Fujii, T.; Yamazaki, T.; Shimada, H.; Arisawa, M. A new methionine antagonist that has antifungal activity: mode of action. *J. Antibiot. (Tokyo)* **1994**, *47*, 909–916.
- (9) Jacques, S. L.; Mirza, I. A.; Ejim, L.; Koteva, K.; Hughes, D. W.; Green, K.; Kinach, R.; Honek, J. F.; Lai, H. K.; Berghuis, A. M.; Wright, G. D. Enzyme-assisted suicide: molecular basis for the antifungal activity of 5-hydroxy-4-oxonorvaline by potent inhibition of homoserine dehydrogenase. *Chem. Biol.* **2003**, *10*, 989–995.
- (10) Yamaguchi, M.; Yamaki, H.; Shinoda, T.; Tago, Y.; Suzuki, H.; Nishimura, T.; Yamaguchi, H. The mode of antifungal action of (S)-2-amino-4-oxo-5-hydroxypentanoic acid, RI-331. *J. Antibiot. (Tokyo)* **1990**, *43*, 411–416.
- (11) Davies, G. M.; Barrett-Bee, K. J.; Jude, D. A.; Lehan, M.; Nichols, W. W.; Pinder, P. E.; Thain, J. L.; Watkins, W. J.; Wilson, R. G. (6S)-6-Fluoroshikimic acid, an antibacterial agent acting on the aromatic biosynthetic pathway. *Antimicrob. Agents Chemother.* **1994**, *38*, 403–406.
- (12) Ejim, L. J.; D'Costa, V. M.; Elowe, N. H.; Loredó-Ostí, J. C.; Malo, D.; Wright, G. D. Cystathionine  $\beta$ -lyase is important for virulence of *Salmonella enterica* serovar typhimurium. *Infect. Immun.* **2004**, *72*, 3310–3314.
- (13) Galan, J. E.; Nakayama, K.; Curtiss, R., III. Cloning and characterization of the *asd* gene of *Salmonella typhimurium*: use in stable maintenance of recombinant plasmids in *Salmonella* vaccine strains. *Gene* **1990**, *94*, 29–35.
- (14) Garmory, H. S.; Brown, K. A.; Titball, R. W. *Salmonella* vaccines for use in humans: present and future perspectives. *FEMS Microbiol. Rev.* **2002**, *26*, 339–353.
- (15) Yang, Z.; Pascon, R. C.; Alspaugh, A.; Cox, G. M.; McCusker, J. H. Molecular and genetic analysis of the *Cryptococcus neoformans* MET3 gene and a met3 mutant. *Microbiology* **2002**, *148*, 2617–2625.
- (16) Fritz, R.; Lanen, C.; Colas, V.; Leroux, P. Inhibition of methionine biosynthesis in *Botrytis cinerea* by the anilinopyrimidine fungicide pyrimethanil. *Pestic. Sci.* **1997**, *49*, 40–46.
- (17) Zhang, J. H.; Chung, T. D.; Oldenburg, K. R. A simple statistical parameter for use in evaluation and validation of high throughput screening assays. *J. Biomol. Screening* **1999**, *4*, 67–73.
- (18) Clausen, T.; Huber, R.; Laber, B.; Pohlenz, H. D.; Messerschmidt, A. Crystal structure of the pyridoxal-5'-phosphate dependent cystathionine beta-lyase from *Escherichia coli* at 1.83 Å. *J. Mol. Biol.* **1996**, *262*, 202–224.
- (19) Belfaiza, J.; Parsot, C.; Martel, A.; de la Tour, C. B.; Margarita, D.; Cohen, G. N.; Saint-Girons, I. Evolution in biosynthetic pathways: two enzymes catalyzing consecutive steps in methionine biosynthesis originate from a common ancestor and possess a similar regulatory region. *Proc. Natl. Acad. Sci. U.S.A.* **1986**, *83*, 867–871.
- (20) Breiting, U.; Clausen, T.; Ehlert, S.; Huber, R.; Laber, B.; Schmidt, F.; Pohl, E.; Messerschmidt, A. The three-dimensional structure of cystathionine beta-lyase from *Arabidopsis* and its substrate specificity. *Plant Physiol.* **2001**, *126*, 631–642.
- (21) Clausen, T.; Huber, R.; Messerschmidt, A.; Pohlenz, H. D.; Laber, B. Slow-binding inhibition of *Escherichia coli* cystathionine  $\beta$ -lyase by L-aminoethoxyvinylglycine: a kinetic and X-ray study. *Biochemistry* **1997**, *36*, 12 633–12 643.
- (22) Lightcap, E. S.; Silverman, R. B. Slow-binding inhibition of gamma-aminobutyric acid aminotransferase by hydrazine analogues. *J. Med. Chem.* **1996**, *39*, 686–694.
- (23) Morrison, J. F.; Walsh, C. T. The behavior and significance of slow-binding enzyme inhibitors. *Adv. Enzymol. Relat. Areas Mol. Biol.* **1988**, *61*, 201–301.
- (24) Marshall, C. G.; Zolli, M.; Wright, G. D. Molecular mechanism of VanHst, an  $\alpha$ -ketoacid dehydrogenase required for glycopeptide antibiotic resistance from a glycopeptide producing organism. *Biochemistry* **1999**, *38*, 8485–8491.
- (25) Leatherbarrow, R. J. *Grafit*, version 4.0; Erithacus Software Ltd: Staines, U.K., 2000.
- (26) Bodansky, M.; Bodansky, A. *The Practice of Peptide Synthesis*; Springer-Verlag: New York, 1984.
- (27) Erlanger, B.; Brand, E. Optical rotation of peptides. I. Glycine and alanine dipeptides. *J. Am. Chem. Soc.* **1951**, *73*, 3508–3510.
- (28) Pflugrath, J. W. The finer things in X-ray diffraction data collection. *Acta Crystallogr., Sect. D* **1999**, *55*, 1718–1725.
- (29) Murshudov, G. N.; Vagin, A. A.; Dodson, E. J. Refinement of macromolecular structures by the maximum-likelihood method. *Acta Crystallogr., Sect. D* **1997**, *53*, 240–255.
- (30) Murshudov, G. N.; Vagin, A. A.; Lebedev, A.; Wilson, K. S.; Dodson, E. J. Efficient anisotropic refinement of macromolecular structures using FFT. *Acta Crystallogr., Sect. D* **1999**, *55*, 247–255.
- (31) Pannu, N. S.; Murshudov, G. N.; Dodson, E. J.; Read, R. J. Incorporation of prior phase information strengthens maximum-likelihood structure refinement. *Acta Crystallogr., Sect. D* **1998**, *54*, 1285–1294.
- (32) Winn, M. D.; Isupov, M. N.; Murshudov, G. N. Use of TLS parameters to model anisotropic displacements in macromolecular refinement. *Acta Crystallogr., Sect. D* **2001**, *57*, 122–133.
- (33) Emsley, P.; Cowtan, K. Coot: model-building tools for molecular graphics. *Acta Crystallogr., Sect. D* **2004**, *60*, 2126–2132.
- (34) Laskowski, R. A.; MacArthur, M. W.; Moss, D. S.; Thornton, J. M. PROCHECK: A program to check the stereochemical quality of protein structures. *J. Appl. Crystallogr.* **1993**, *26*, 283–291.
- (35) DeLano, W. L. *The PyMOL Molecular Graphics System*; DeLano Scientific: San Carlos, CA, 2002.

JM061132R